DOI:https://doi.org/10.52756/ijerr.2024.v44spl.005 ***Int. J. Exp. Res. Rev.*, Vol. 44: 51-65(2024)**

Original Article | *Peer Reviewed* | *Open Access*

International Journal of Experimental Research and Review (IJERR)

ISSN: 2455-4855 (Online)
www.iaph.in

ISSN 2455-4855

An Effective PDE-based Thresholding for MRI Image Denoising and H-FCM-based Segmentation

Sreedhar Kollem[1], Samineni Peddakrishna[2]*, P Joel Josephson[3], Y Rama Lakshmanna[4], Garaga Srilakshmi[5] and Sridevi Cheguri[6]

[1]Department of ECE, School of Engineering, SR University, Warangal, Telangana, India-506371; [2]School of Electronics Engineering, VIT-AP University, Amaravati, Andhra Pradesh, India-522237; [3]Department of ECE, Malla Reddy Engineering College, Secunderabad, Telangana, India-500100; [4]Department of ECE, SRKR Engineering College, Bhimavaram, Andhra Pradesh-534204; [5]Department of ECE, Aditya College of Engineering and Technology, Surampalem, Andhra Pradesh, India-533437; [6]Department of ECE, St. Martins Engineering College, Secunderabad, Telangana, India-500100

E-mail/Orcid Id:

SK, ksreedhar829@gmail.com, https://orcid.org/0000-0002-9203-0404; *SPK,* krishna.samineni@gmail.com, https://orcid.org/0000-0002-5925-8124; *PJJ,* joeljosephsonp@gmail.com, https://orcid.org/0000-0003-1804-8080; *YRL,* yrljohson@gmail.com, https://orcid.org/0000-0002-5356-477X; *GS,* srilakshmi1853@gmail.com, https://orcid.org/0009-0005-5254-7766; *SC,* cheguri.sridevi@gmail.com, https://orcid.org/0009-0004-2714-7245

Article History:

Received: 08th Apr., 2024
Accepted: 18th Oct., 2024
Published: 30th Oct., 2024

Keywords:

Adaptive Haar Wavelet Transform, Fuzzy C-means Clustering, Generalized cross-validation, Image denoising, Partial differential equation

How to cite this Article:

Sreedhar Kollem, SamineniPeddakrishna, P Joel Josephson, Y Rama Lakshmanna, Garaga Srilakshmi and Sridevi Cheguri (2024). An Effective PDE-based Thresholding for MRI Image Denoising and H-FCM-based Segmentation. *International Journal of Experimental Research and Review*, *44*, 51-65.
DOI:10.52756/ijerr.2024.v44spl.005

Abstract: Image denoising and segmentation play a crucial role in computer graphics and computer vision. A good image-denoising method must effectively remove noise while preserving important boundaries. Various image-denoising techniques have been employed to remove noise, but complete elimination is often impossible. In this paper, we utilize Partial Differential Equation (PDE) and generalised cross-validation (GCV) within Adaptive Haar Wavelet Transform algorithms to effectively denoise an image, with the digital image serving as the input. After denoising, the image is segmented using the Histon-related fuzzy c-means algorithm (H-FCM), with the processed image serving as the output. The proposed method is tested on images exposed to varying levels of noise. The performance of image denoising and segmentation techniques is evaluated using metrics such as Peak Signal-to-Noise Ratio (PSNR) of 77.42, Mean Squared Error (MSE) of 0.0011, and Structural Similarity Index (SSIM) of 0.7848. Additionally, segmentation performance is measured with a sensitivity of 99%, specificity of 98%, and an accuracy of 98%. The results demonstrate that the proposed methods outperform conventional approaches in these metrics. The implementation of the proposed methods is carried out on the MATLAB platform.

Introduction

The transmission of multimedia substances such as digital images has recently been widely developed on the internet (Islam et al., 2016). In hyperspectral images (HSI), the eminence of the image is significantly affected by the occurrence of noise. So, denoising is carried out as a spatial preprocessing procedure which is used to develop the image eminence for data analysis (Aswathy et al., 2015). Image denoising is a common problem in image processing. As a result of several types of noise, digital images are often blurry. In digital image processing, noise is a quantity that can change the experimental value from its original value (Bhandari et al., 2016). The digital image is somewhat distorted by noise during the transmission or acquisition of the image. The foremost objective of image denoising is to evaluate the original image, such as the edges, textures, and fine details of its noise-degraded analysis. In many image processing systems, image denoising is a crucial preprocessing step, and the exploration of function is an essential challenge (Shaoping et al., 2016). Additionally, it is utilized to enhance the prominence of images to help visual assessment. MRI denoising is a difficult problem in medical image processing because of the improbability

***Corresponding Author:** krishna.samineni@gmail.com

of resources and the allocation of noise (Ai, Danni et al., 2015; Gautam et al., 2022; Jain et al., 2023; Goel et al., 2023; Himabindu et al., 2024).

Gaussian is typically used for noise recognition. Magnetic resonance (MR) images with noise have been found to be in Rician (Phophalia et al., 2014, 2016). Additionally, several research works for image denoising have recently been predicted. However, the challenge is still seen in the latest studies. Usually, a linear representation like a Gaussian filter is used to diminish the noise (Malini et al., 2015). The flat area of the images is where these procedures perform best. One of the main advantages of the linear procedure is its relatively high computing efficiency. However, it is difficult for these procedures to reconstruct the entire original image and achieve the optimal denoising properties using only the local information of the observed image (Feng et al., 2015). Additionally, non-linear representation is employed to maintain limits that are superior to those of the linear model (Jalab et al., 2015; Naresh and Peddakrishna, 2023).

Here, several additional algorithms are also employed to eliminate noise. One approach that derives from thresholding is the multiresolution denoising algorithm. It is used to keep the residual as unaltered (hard-thresholding) or decrease it to the threshold value by setting all wavelet coefficients to zero in the chosen threshold value (Huang et al., 2015, 2016, 2014). Here, the Gaussian smoothing filter has become the standard. This type of local averaging procedure is to eliminate noise with structural information such as anatomical limitations. The actual noise has a huge impact on how the denoising process is presented. The impact of noise on several procedures, including image segmentation. Image segmentation is essential and significant for computer visualization, pattern identification, and medical image processing. The foremost intention of image segmentation is to divide an image mechanically or semi-automatically as non-overlapping regions. Every area is standardized by some uniqueness like intensity or texture (Feng and Bhandari, 2016). The anisotropic diffusion function is a characteristic of the partial differential equation used for noise reduction and the preservation of image features, including edges. The work introduces a tangent sigmoid diffusion coefficient and an adaptive threshold value, which results in accelerated convergence (Kollem, 2024). An approach to image denoising utilizing a diffusivity function-based partial differential equation that takes advantage of the statistical features of the observed noisy images. This model employs a Quaternion Wavelet Transform, which generates the various coefficients of a noisy image. The soft threshold function is employed to enhance the generalized cross-validation function, which identifies the optimal threshold value. The ideal threshold value subsequently regulates the diffusion process through a novel diffusivity function. They present the fourth-order partial differential equation diffusivity function, a distinctive diffusion coefficient that surpasses previous methods in noise reduction and edge preservation (Kollem, 2023).

This work aims to create an efficient approach for image denoising and segmentation that addresses the shortcomings of current strategies with respect to noise elimination and boundary preservation. The proposed approach utilizes Partial Differential Equations (PDE) and generalised cross-validation (GCV) in the adaptive Haar Wavelet Transform to markedly diminish noise while preserving the image's structural integrity. The Histon-related fuzzy c-means algorithm (H-FCM) is employed for segmentation to improve the precision of image segmentation, especially in noisy conditions. The primary objective is to achieve enhanced performance in denoising quality and segmentation accuracy, evidenced by superior performance measures including PSNR, SSIM, MSE, sensitivity, specificity, and accuracy relative to traditional approaches.

Literature Survey

This section discusses the image denoising and segmentation techniques that various authors have proposed. The approach suggested by Kollem et al. (2022) uses a Quaternion Wavelet Transform to create the various noisy image coefficients, an improved generalized cross-validation function to produce the ideal threshold value, and a new diffusivity function to regulate the diffusion process. This approach is not superior in terms of eliminating noise and maintaining sharp edges.

An approach to denoising that is based on anisotropic diffusion processes has been proposed by Ally et al. (2021). To effectively preserve edges, contours, and textures, this approach's divergence and regularization terms include a diffusion kernel that depends on the evolving image and its gradient magnitude. In MRI images, this technique causes distracting artifacts.

Lotfi et al. (2022) have presented a method that contains a partial differential equation, numerical approaches, and the Perona-Malik equation to eliminate noise in an image. This method reduces the size of the original problem by decomposing it into a set of smaller problems, each of which is addressed differently. Being unidirectional also eliminates the necessity for the intricate process of domain decomposition while solving

DOI:https://doi.org/10.52756/ijerr.2024.v44spl.005

the equations. The Perona-Malik methods produce the desired denoised results using meshless techniques.

An approach to maintaining the edges of the image has been suggested by Rafsanjani et al. (2022). This approach combines efficient diffusion-based technology with residual feedback. The suggested method employs residual feedback and the localization of the noisy pixels, and it is carried out in two stages. There is a loss of detail in the image and problems with large gradients when using this technique.

Abdellahoum et al. (2021) have come up with a method that uses a cooperative approach and improved fuzzy c-means. This cooperation is controlled by a multi-agent system that makes it possible to choose the best metaheuristics parameters automatically. The disadvantage, which results in a reduction in the segmentation accuracy, is the improper selection of clusters and their initialization.

Kollem et al. (2020) developed a method that combines centroid optimization using the elephant herding approach with Atanassov's intuitionistic fuzzy set Histon-based fuzzy clustering method. This optimization strategy is used to choose clusters effectively. The instability in clustering is a result of the method's use of clan updating and separation operators.

The fuzzy c-means clustering was proposed by Mishro et al. (2020) to segment brain MR images. This method's algorithm for segmenting brain tissue is a type-2 adaptive spatial fuzzy c means technique. The fixed value of the fuzzifier employed in fuzzy c-means, which introduces uncertainty in regulating the fuzziness of the extracted clusters, is a downside of this method.

Zhang et al. (2019) demonstrated image segmentation. using a hybrid approach Using an evolutionary algorithm to find improved clustering solutions, this technique first generates a random population of initial clustering solutions at random then, at each iteration, the FCM technique is applied to each of these solutions to generate its segmentation result.

Liu et al. (2016) established an image denoising process by means of developing the sparse depiction of boundaries and the multidirectional reduction. The augmentation of sparsity was accomplished by means of implementing directionlet transforms, which are created by the directions of boundaries. Here, the created directionlet transforms are carried out in dissimilar directions for every pixel. They acquired numerous dissimilar estimations, which were the finest. The concluding denoised output was acquired by means of a weighted averaging of entity evaluation.

Saeid Saryazdiet al. (2016) specify that the Perona-Malik (PM) dispersion coefficient was investigated by flux. According to the investigation, the PM flux of the section, where the gradient magnitude was superior to the smoothing threshold, is directly related to unwanted blurring consequences and border dislocation. The image was separated into three segments to tackle those problems that are derived from the gradient magnitude: a section where the gradient was lesser than the smoothing threshold, a section where the gradient was among the smoothing threshold and modulation position of flux, and a section where the gradient magnitude was superior to modulation position. They describe the circumstances that are measured in those three segments. After that, the conditions are satisfied by a calculated dispersion coefficient.

Khan et al. (2016) presented an innovative impulse noise recognition algorithm that is derived from noise proportion assessment and a mixture of K-means clustering and Non-Local Means related filter (NEK-NLM). Luo-statistic has engaged a nonlocal means-related estimator. The uniqueness of the process is handling the establishment of the preprocessing step of noise proportion assessment before noise recognition, which is used to pick the appropriate limitation for the noise recognition algorithm (Xiaoyan et al., 2016). The nonlocal-means estimator was implemented in the noise filtering phase to re-establish the noisy pixels for their definite values. In actual world datasets, the design illustrates that the impulse noise is detached efficiently.

Zhang et al. (2015) established the anticipated algorithm, which employs partial differential equations (PDE) and generalized cross-validation (GCV) theory in the tetrolet transform field. It is used to reduce noise in an image. The noisy image was analyzed using the Tetrolet transform, and the finest denoising threshold in the Tetrolet transform domain was determined using the GCV theory. Subsequently, the inverse tetrolet transform was employed to the customized tetrolet transform coefficients to acquire a preliminary denoising image. The PDE representation was employed to diminish the block consequence that occurs by means of tetrolet transform to decrease noise and maintain the border information (Wei Xie et al., 2016). The anticipated image denoising algorithm was evaluated by way of five comparable image denoising algorithms such as wavelet transform combined with PDE, contourlet transforms combined with PDE and curvelet transform combined PDE, shearlet transform combined with PDE and tetrolet transform combined with PDE correspondingly.

DOI:https://doi.org/10.52756/ijerr.2024.v44spl.005

Contributions

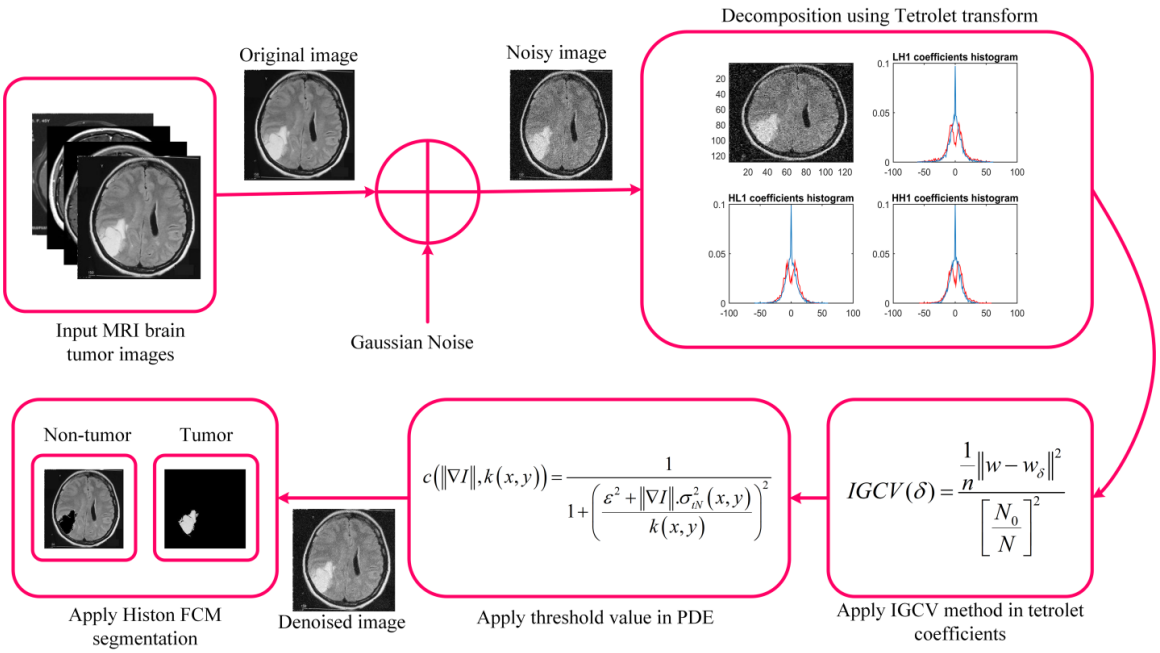

Figure 1. Architecture of the Proposed PDE Threshold Function-Based Image Denoising and Histon FCM-Based Segmentation.

Problem Definition

A review of the research shown above has some of the problems with recent image denoising and segmentation methods as follows:

The newly developed diffusivity function in (Kollem et al., 2022) suppresses the image details.

In this approach, the divergence and regularization terms include a diffusion kernel that gives blurry images (Ally et al., 2024).

This method employs effective diffusion-based technology with residual feedback, although there is a loss of image detail and issues with large gradients when employing this method (Rafsanjani et al., 2022).

This method makes use of a cooperative approach and an improved fuzzy c-means algorithm, both of which result in an incorrect selection of clusters and initialization of those clusters (Abdellahoum et al., 2021).

This methodology combines Atanassov's intuitionistic fuzzy set Histon-based fuzzy clustering algorithm with the elephant herding strategy. Border displacement occurs as a result of clustering instability (Kollem et al., 2020).

This technique uses a type-2 adaptive spatial fuzzy c means algorithm to segment brain tissue. One drawback of this approach is the fixed value of the fuzzifier used in fuzzy c-means, which introduces uncertainty in controlling the fuzziness of the retrieved clusters (Mishro et al., 2020).

Therefore, these limitations inspired us to create the proposed approach, in which all of the problems are fixed.

The following are the contributions to address the limitations identified in Section 2.

The tetrolet transform is used as an application to extract the image into low and high-frequency coefficients.

Improved generalized cross-validation is used to obtain the optimal threshold value.

A new diffusion coefficient is used in the partial differential equation based on Improved generalized cross-validation for image denoising.

An improved Histon-based fuzzy c means clustering is proposed for image segmentation.

Proposed Methodology

In this part, we have addressed the implementation of the proposed method. The proposed approach for image denoising has the primary objective of removing noise while preserving boundaries' integrity. The primary objective of the proposed image segmentation is to prevent over-segmentation and noise sensitivity. The following is a description of Figure 1: The preliminary MRI images of the brain tumor, which were obtained from the reference resource known as BraTS2021(Baid et al., 2021). The tetrolet transform is used to decompose a noisy image into low- and high-frequency coefficients. A threshold approach is used to eliminate noisy image coefficients. In the tetrolet transform, the GCV method is utilized to locate the finest denoising threshold value at each scale level. The proposed partial differential equation method produces a denoised image using an optimal threshold value. With the help of a Histon-related

DOI:https://doi.org/10.52756/ijerr.2024.v44spl.005

fuzzy c-means method, the denoised image is segmented (Binge Cui et al.,2016). As a result, we get segmented images as output. The sensitivity, specificity, and segmentation accuracy of PSNR, SSIM, MSE have all been used to calculate the performance of the proposed approaches. The proposed method is briefly discussed below:

Tetrolet transform

Using partial differential equations (PDEs) and generalized cross-validation (GCV) in the tetrolet transform, a novel image-denoising algorithm is expected to be presented in this article. The proposed algorithm's complexity is reduced by using the tetrolet transform's admirably sparse representation. Based on tetrominoes, the Tetrolet Transform is a novel adaptive wavelet transform in the Haar category. In general, the tetrominoes encompass four equal-sized squares, and each boundary is linked to another.

Consider the following scenario: for each N*N image, if the value of N is even, then the image may be enclosed using only the five fundamental tetrominoes. At the beginning of the process, the image is divided into 4*4 blocks at each stage of the tetrolet transform field. After that, using a technique called tetrominoes segmentation, which is determined by the uniqueness of the block's geometry, four sections are extracted. The input image is $U=(u[i,j])_{i,j=0}^{N-1}$ and where $N=2^J\left(J\in N\right)$. The equations for the low-frequency and high-frequency coefficients can be found below.

$$u_l=\left(u_l\left[i,j\right]\right)_{i,j=0}^{\frac{N}{2}-1} \text{ and}$$

$$u_l\left[i,j\right]=\sum_{\left(i^{'},j^{'}\right)\in U_{i,j}}\eta\left[0,K\left(i^{'},j^{'}\right)\right]u\left[i^{'},j^{'}\right] \quad (1)$$

The low-frequency coefficients are calculated with Equation (1). The matrix of the tetrolet transform is denoted by the letter $K\left(i^{'},j^{'}\right)$, while the coefficient of the tetrolet transform [28] is denoted by the letter η.

$$u_h=\left(u_h\left[i,j\right]\right)_{i,j=0}^{\frac{N}{2}-1} \text{ and}$$

$$u_h\left[i,j\right]=\sum_{\left(i^{'},j^{'}\right)\in U_{i,j}}\eta\left[l,K\left(i^{'},j^{'}\right)\right]u\left[i^{'},j^{'}\right] \quad (2)$$

The high-frequency coefficients are calculated with Equation (2). Where $l=1,2,3$ denotes the various components that make up the high-frequency coefficients.

The steps involved in the tetrolet transformation (Kollem et al., 2019) are outlined below.

Input: Image $U=(u[i,j])_{i,j=0}^{N-1}$ and where $N=2^J\left(J\in N\right)$

Step-1: During this process stage, the image is divided into 4*4 blocks.

Step-2: Equations (1) through (2) are used in the tetrolet transform, which allows for the acquisition of high-frequency and low-frequency coefficients. Obtaining the most sparsetetrolet depiction in each block is desirable when the tetrolet coefficient is insignificant.

Step 3:2*2 blocks are used to reorder the high-frequency and low-frequency coefficients.

Step 4: Accumulation is performed using the high-frequencytetrolet coefficients.

Step 5: The low-frequency tetrolet coefficients are found by going through steps 1–4.

Output: Decomposed image $\tilde{u}$

The GCV algorithm is used to establish the finest denoising threshold value at every scale level in the tetrolet field.

Improved generalized cross validation (IGCV)

In the wavelet field, the IGCV method is used to compute the finest denoising threshold and is also utilized in partial differential equations. Here, $arg\ min\ IGCV\left(\delta\right)=arg\ min\ \ MSE\left(\delta\right)\ \ if\ \ N>\infty$ verifies the algorithm. The finest denoising threshold is acquired by means of the RGCV method, which is used to evaluate MSE. This process is used to maintain the comprehensive uniqueness of the innovative image. The GCV task is used to compute the finest denoising threshold in the wavelet field. The GCV principle is used to establish the finest denoising threshold to accomplish a superior denoised image in the tetrolet transform field.

The input of algorithm is

$$y=f+\in \quad (3)$$

$f-$ Unknown deterministic structure data.

$\in$ - *noise*

$y-observation$

$$w=\nu+\omega \quad (4)$$

$\nu=Wf$ - contains the wavelet co-efficient of original data, $\omega=W\in$ - Noise co-efficient

$w=Wy$

Here, we select the subsequent GCV task for the threshold value:

$$GCV(\delta)=\frac{\frac{1}{n}\left\|w-w_\delta\right\|^2}{\left[\frac{N_0}{N}\right]^2} \quad (5)$$

N -total number of wavelet co-efficient

DOI:https://doi.org/10.52756/ijerr.2024.v44spl.005

N_0–the number of this coefficient that was replaced by zero.

This threshold selection is asymptotically finest for a huge quantity of wavelet coefficients. The least $Gcv(\delta)$ also reduces the mean square error task (or risk function) $R(\delta)$ where,

$$R(\delta) = \frac{1}{N}\|w\delta - v\|2 \quad (6)$$

E-denotes the expectation operator in eq (5)

$$EGCV(\delta) = ER(\delta) + \sigma^2 \quad (7)$$

σ^2 -Denotes the standard deviation

The higher threshold value contains additional noise. The threshold choice process such as the "universal threshold" of Donoho and Johnstone is specified as, $\delta = \sqrt{2\log(N)\sigma}$ (8)

Suppose that *X* is an innovative image and *Y* is noisy image, then tetrolet decomposes *Y* whose coefficient encompasses low frequency as *Y* Low, high frequency coefficients *Y* High and allocation of preferred covering *YC*. Afterward, *Y* Low and YC are retrained and *Y* High is customized by means of threshold which is derived from GCV principle. Suppose that if the image is decomposed into three stages by means of a tetrolet transform, then we identify a *matrix m * ny*$^l_{ij}$ = $y^l_{high}[i,j]$ through the high-frequency coefficients of the row *i* column *j* in stage l. In the GCV principle, the soft threshold is situated as δ in advance and acquires $s_{ij} = y^{\,l}_{ij}$ which is the consequence of the threshold. Soft threshold task is specified as,

$$S_{ij} = \begin{cases} 0 & if \left|y_{ij}^{\,1}\right| < \delta \\ Y_{ij}^{\,1} - \delta & otherwise \end{cases} \quad (9)$$

In the tetrolet field, the GCV task is specified as

$$GCV(\delta) = \frac{\frac{1}{N}\left\|y_{ij}^{\,1} - y_{ij}^{\,1}\right\|^2}{\left[\frac{N_0}{N}\right]^2} \quad (10)$$

$y_{ij}^{\,1}$ is the co-efficient after threshold processing and N=*m*n, and* N_0=*N-S*

S-Number of coefficients that are set to after threshold processing,

In this investigational image, the standard deviation of Gaussian white noise is 20 and mean is *0*. The three-level tetrolet transform is used to decompose the image. The *GCV (δ)* of the tetrolet coefficient is used to evaluate *MSE(δ)* in dissimilar thresholds. The GCV task is an approximate assessment for *MSE(δ)*. The threshold is equivalent to the least value of *GCV (δ),* which is the best denoising threshold. The finest threshold is acquired by means of the subsequent equation:

$$\delta_{opt} = \arg\min GCV(\delta) \quad (11)$$

Partial differential equation (PDE)

The Fast Fourier Transform (FFT) process is a systematic procedure for arithmetical investigation. It supplies the estimated investigation for partial differential equations (PDE), which is usually premeditated by means of the development. It is also known as the basis process, which is employed to compute the unidentified coefficients. Afterward, we implement the FFT process to partial differential equations, which is specified as,

$$\frac{\partial u}{\partial t} = c^2\left(\frac{\partial^2 u}{\partial x^2} + \frac{\partial^2 u}{\partial y^2}\right) + E(x,y) \quad (12)$$

It is used to diminish the number of spatial variables in anticipation of a two-position boundary or preliminary value difficulty, which is resolved by a standard process. Here, FFT is used to divide the variables to expand the partial differential equation. Due to higher degree, the PDE of Fourth order is an aid for diminution and division. It is extra flexible in the circumstance and division of variables; therefore, the recognition is simple and noticeable and diminishes the noise coefficients. The identical division is used for the edge circumstances. But, it is only relevant for the resolute or limited values through the mixture of FFT. Consider $\Theta = \Theta(r,t)$ the field variable (e.g., temperature or concentration), and L is a differential operator encompassing additional spatial derivatives and a time derivative. Numerous Partial differential equations are depicted in the beneath equation,

$$L\Theta = s(r) \quad (13)$$

Here *S(r)* is a task that indicates the dimension location. The differential operator is said to be linear *i.*

$$L(a_1\Theta_1 + a_2\Theta_2) = a_1 L\Theta_1 + a_2 L\Theta_2 \quad (14)$$

Here a_1 *and* a_2 are constants $\Theta_1(r,t)$ *and* $\Theta_2(r,t)$ that are tasks which are not essentially an explanation $L\Theta = s(r)$. We can concern the edge values which must satisfy the limit circumstances which are the divided values in identical circumstances to investigation. It provides the identical occurrence.

Consider the following PDE,

$$\left(\frac{\partial^2\Theta}{\partial x^2} + \frac{\partial^2\Theta}{\partial y^2}\right) = 0 \quad (15)$$

With the boundary conditions,

$$\Theta(0,y) = 0, \Theta(1,y) = 0$$
$$\Theta(x,0) = f_0(x), \Theta(x,1) = f_1(x) \quad (16)$$

DOI:https://doi.org/10.52756/ijerr.2024.v44spl.005

The solution can be written in a series expansion as,

$$\Theta(x,y)=\sum_{n=1}^{\infty}C_n(y)\,\Phi_n(x) \qquad (17)$$

In this equation $\Phi_n(x)$ are given by: $\Phi_n(x)=\sqrt{2},\sin(n\pi x)$, n-1, 2,….

Here, we have integrated the Haar wavelet with mathematics. The Haar wavelet is a progression of rescaled "square-shaped" task that consists of constructing a wavelet or source. The Haar wavelet's mother wavelet task of $\delta(t)$ is specified as,

$$\delta(t)=\begin{cases}1 & 0\le t\le 1/2\\ -1 & 1/2\le t\le 1\\ 0 & otherwise\end{cases} \qquad (18)$$

Its scaling function $\phi(t)$ can be described as

$$\phi(t)=\begin{cases}1 & 0\le t\le 1\\ 0 & other\,wise\end{cases} \qquad (19)$$

This least compression proportion accomplishes the Harr wavelet coefficients with DWT progression. Therefore, the enhanced CR optimizes harr coefficients with optimization procedure. In Haar wavelet, the GCV algorithm is used to establish the finest denoising threshold value at every scale stage. It is an adaptive Haar wavelet transformation for image sparse depiction that encompasses the uniqueness of the geometric arrangement and superior energy concentrating capability (Mittal, 2023). The foremost problem in the Haar wavelet is blocking the object, and GCV will be employed to choose the finest denoising threshold in the anticipated algorithm. The threshold denoising algorithm is trendy in image proposals because it is easy and competent in several circumstances. On the other hand, the existing denoising threshold choice process is relying on noise statistic possessions like variance. Regrettably, the precise arithmetical possessions of noise are normally unidentified in definite problems. Therefore, the denoising threshold is complicated to evaluate without deliberate arithmetical possessions of noise. GCV is extensively implemented in image processing, establishing an effectual arithmetical process to evaluate finest denoising threshold value. The denoised image is segmented by means of the Histon-related fuzzy C-means algorithm (H-FCM).

Histon based FCM

Image analysis is removing information from an image. Image segmentation is a fundamental step in automatic pictorial model identification and picture investigation, which is the major complicated function in image processing. It is the progression of dividing a digital image into numerous sections or clusters and is employed for establishing objects of concentration and limitations such as lines and curves in an image. A group of pixels invents every section. The compound image is used to discover the function of supplementary image processing functions like segmentation, attribute removal, machine object identification, etc. Some of the necessities of high-quality color image segmentation are as follows: A solitary section in a segmented image does not include dissimilar colors, and a related section includes an identical color that does not encompass additional markers. The entire noteworthy pixels contain the identical labeled section. The force of the section is logically consistent. Color image segmentation is constructive in numerous functions. It is feasible to recognize the section of concentration and objects in the scene from the segmentation consequences, which assist the successive image investigation. Fuzzy-related procedures have an increasing reputation in the area ofcolor image segmentation. The anticipated process does not necessitate prior information regarding the number of objects in an image and computes the threshold value mechanically necessary for segmentation. Segmentation of compound color image is measured, which unites the feature of FCM and A-IFS procedure for to accomplish enhanced presentation. This process is used to compute association values by means of FCM and A-IFS Histon to manipulate the number of clusters. Finally, it utilizes an irregularity catalogue to obtain the best threshold values for segmentation. The FCM algorithm is implemented to discover the association values as depicted in the preceding segment. The non-association values and the irregularity catalog are established by means of A-IFS Histon process. Irregularity catalogue is employed for isolating the section. In conclusion, section amalgamation is made to accomplish enhanced section related segmentation which is reliant on color.

Generally, digital images are distinguished by means of inherent imprecision or ambiguity of grey values. This type of uncertainty is maintained by section limitations, where it is greatly complicated to encompass an obvious separation of boundaries. Clustering procedures are derived from FCM, which broadly contracts with uncertainty. Intuitionist fuzzy set theory is the trendy procedure that is utilized in image processing. Additionally, instinctive methods are used to depict the inherent uncertainty in images. Intuitionist fuzzy sets are anticipated using Atanassov, which is appropriate for representing the uncertainty from inaccurate information. These are distinct by means of two feature tasks, the association task and the non-association task. Association

DOI:https://doi.org/10.52756/ijerr.2024.v44spl.005

task provides a quantity of belongingness of a component to the creation of IFS and non-association task provides the quantity of non-belongingness. The HFCM depiction of images is specified by means of $I=\{gij,\mu I(gij),vI(gij)\}$, $i=1,\ldots,M;\ j=1,\ldots,N.$

$I=\{g_{ij},\mu_I(g_{ij}),v_I(g_{ij})\}, i=1.....,M;j=1,\ldots\ldots,N\ldots\ldots\ldots\ldots(1)$ (20)

g_{ij}-gray values in an image of size M *N, $\mu_I(g_{ij})$-degree of membership.

$v_I(g_{ij})$- degree of non-membership.

The membership value is specified by means of the standardized intensity values at every pixel position. The anticipated method is diverging from the computation of association values. In the anticipated procedure, the FCM algorithm is implemented to discover the association values rather than the standardized intensity values because the association values with the FCM algorithm are specified below:

An image *'I'* of size *p x q* with '*n*' number of clusters is considered for analysis.

$$I=\begin{bmatrix}(c1,c2c3_{(1*1)} & L & (c1,c2c3)_{(1*q)}\\ M & O & M\\ (c1,c2c3)_{(p*1)} & L & (c1,c2c3)_{(p*q)}\end{bmatrix} \quad (21)$$

The objective function, J_{FCM} of the image '*I*' is first initialized to zero,

$$J_{FCM(0)}=0 \quad (22)$$

A matrix '*U*' is used to store the membership functions '$\mu x,i$' corresponding to each pixel value.

$$I=\begin{bmatrix}(\mu)_{(1,1)} & (\mu)_{(2,1)} & L & (\mu)_{(n,1)}\\ M & & O & M\\ (\mu)_{(1,0)} & (\mu)_{(2,0)} & L & (\mu)_{(n,0)}\end{bmatrix} \quad (23)$$

The centre 'ϑ_i' of each cluster containing the membership values of each pixel is given by,

$$\vartheta_i=\frac{\sum_{x-1}^{N}\mu_{xi}^{m}z_x}{\sum_{x-1}^{N}\mu_{xi}^{m}} \quad (24)$$

Here $v_i(i=1,2,\ldots, c)$ is the centre of cluster, $\mu_{(x,i)}$ $(x=1,2,\ldots, n,\ i=1,2,\ldots, c)$ is association value and $Z_x = (c_1, c_2, c_3)\ x,\ (x=1,2,\ldots, n)$ is the pixel value and *'m'* is fuzzification limitation which is generally obtained as 2 for soft clustering. The detachment equation is used to discover the distance 'd' from the centre of cluster at each pixel which is specified by,

$$d^2(z_x,v_i)=\left\|z_x-v_i\right\|^2 \quad (25)$$

Using the membership values and Euclidean distance, the objective function is calculated by,

$$\sum_{i=1}^{N}\sum_{i=1}^{c}\mu_{xi}^{m},d^2(z_x,\vartheta)=J_{FCM}(\gamma) \quad (26)$$

Here, *'r'* is the number of iterations. The dissimilarity among the current objective task and the preceding objective task is specified as,

$$Difference=J_{FCM}(\gamma)-J_{FCM}(\gamma-1) \quad (27)$$

Suppose that if this dissimilarity is less than the threshold value, then the clustering is blocked. This threshold value is preferred after creating a widespread analysis of a quantity of images to conclude the iteration. A threshold of superior value is answered in unacceptable clustering for several images. If the dissimilarity exceeds the threshold value, the subsequent iteration is established from step 4. The innovative association task for next iteration is specified as,

$$\mu_{x,i}=\frac{\left(\frac{1}{d^2(z_x\int i)}\right)^{\frac{1}{(m-1)}}}{\sum_{i-1}^{c}\left(\frac{1}{d^2(z_x\int i)}\right)^{\frac{1}{(m-1)}}} \quad (28)$$

The average intensity of the pixels is given by,

$$\mu_l^a(g_{ij})=\sum_{k=l}^{1}\sum_{l=-1}\mu_l(g(i+k)(j+l)h(i+k,j+1)) \quad (29)$$

Where, *'h'* is the filter mask and $\mu_I=\mu_{x,i}$ as found in equation 9. The hesitancy degree, which lies between *0* and *1* are given by,

$$\pi_l(g_{i,j})=(1-\mu_1(g_{i,j})\frac{\left|\mu_l(g_{i,j})\right|-\mu_l^a(g_{i,j})}{\max_{j=1}^{m}(\max_{j=1}^{N}(\left|\mu_l(g_{i,j})-\mu_l^a(g_{i,j})\right|))} \quad (30)$$

The non-membership degree at each pixel location is given by,

$$v_l(g_{ij})=1-\mu_1(g^iij)-\pi_1(g^iij) \quad (31)$$

The A-IFS Histon can be defined as,

$$v_l(g_{ij})=1-\mu_1(g^iij)-\pi_1(g^iij) \quad (32)$$

'g' lies between *0* to *L-1* and $i = \{ R , G, B\}$. *'δ'* represents the impulse function.

$$\mu(m,n)=\exp\left(-0.5\left(\frac{d_r(m,n)}{\sigma}\right)^2\right) \quad (33)$$

σ - Standard deviation of the distance matrix. The total distance of all the pixels in a *PXQ*neighborhood of size *3×3* is given by,

$$d_t(m,n)=\sum_{p\subset P}\sum_{q\subset Q}d(I(m,n)I(p,q)) \quad (34)$$

The Euclidean distance between two pixels, *I (m, n)* and *I (p, q)* is given by,

DOI:https://doi.org/10.52756/ijerr.2024.v44spl.005

$$d_t((m,n).I(p,q)) = \left(\frac{1}{6}\sum_{i(RGB)}\left[(\mu^i(l(m,n)) - \mu^i(l(p,q)))^2 + (\vartheta^i(l(m,n)) - \vartheta^i(l(p,q)))^2 + \pi^i(l(p,q)))^2\right]\right)^{0.5}$$

(35)

After calculating the Euclidean distance, a measure called roughness index is calculated, which is given by,

$$p = 1 - (|f_i(g)| \div |F_i(g)|) \quad (36)$$

Here '$F_i(g)$' is the histogram of the image. In the object section, irregularity catalog is large and it is close to concord. In edge section, this value is diminutive and it is close to zero. Therefore, an irregularity catalogue is valuable in isolating the object section from limitations. Finally, the section amalgamation algorithm is used to modify the segmented output. After considering a quantity of images for investigation,

Results and Discussions

To evaluate the performance of the proposed technique, the classification is to be performed with the aid of the Histon-related fuzzy c means algorithm (H-FCM).Here, the performance is to be measured using Sensitivity, Specificity, and Accuracy.

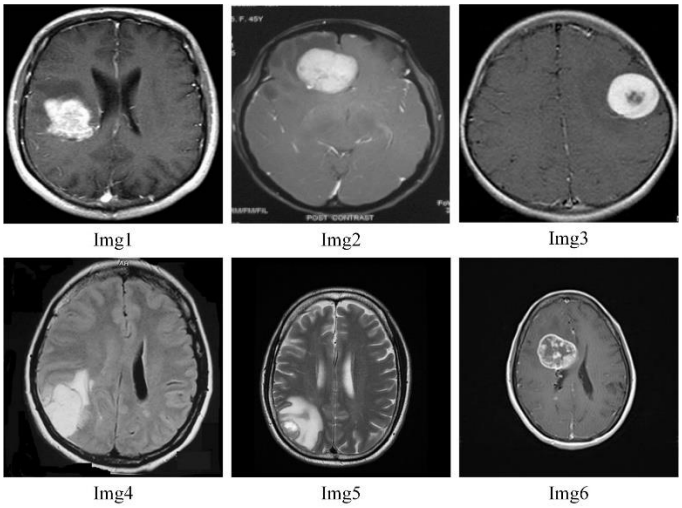

Figure 2.Input Images such as Img1, Img2, Img3, Img4, Img5 and Img6.

In the above section, we have included six input medical images.

Sensitivity

The measure of sensitivity is the proportion of actual positives that are accurately recognized. It relates to the ability of tests to recognize positive results.

$$\text{Sensitivity} = \frac{TP}{(TP + FN)} \quad (37)$$

where TP stands for true positive and FN stands for False Negative

Specificity

The measure of specificity is the extent of negatives that are properly recognized. It relates to the capacity of the test to recognize negative results.

$$\text{Specificity} = \frac{TN}{(TN + FP)} \quad (38)$$

Where TN stands for True Negative and FP stands for False Positive

Accuracy

The accuracy of the proposed method is the ratio of the total number of TP and TN to the total amount of data.

$$\text{Accuracy} = \frac{TN + TP}{(TN + TP + FN + FP)} \quad (39)$$

Discussions

The simulation results of the proposed and existing methods are given below.

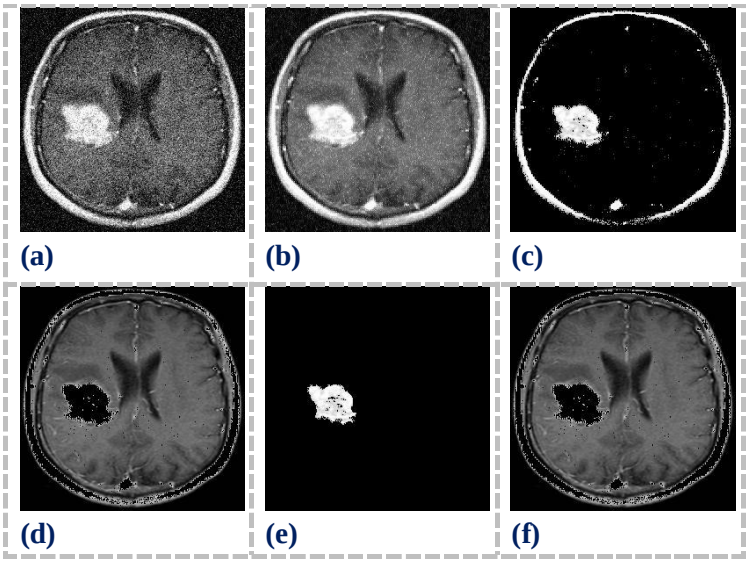

Figure 3. Img1 (A)Noisy Image, (B) Denoised image, (C) Existing K-Means segmented Tumor output, (D) Existing K-Means segmented non-Tumor output, (E) Proposed Histon based FCM segmented tumor output, (F) Proposed Histon based FCM segmented non-tumor output.

Table 1. Truth table for Experimental outcome.

Experimental Outcome	Condition as determined by the Standard of Truth	
	Positive	Negative
Positive	TP	FP
Negative	FN	TN

Performance analysis

In order to evaluate the performance of the proposed technique, the classification is to be performed with the aid of Histon based Fuzzy C-Means Clustering technique here the performance is to be measured by using Sensitivity, Specificity and Accuracy. Table 1 shows performance measures for our proposed work.

DOI:https://doi.org/10.52756/ijerr.2024.v44spl.005

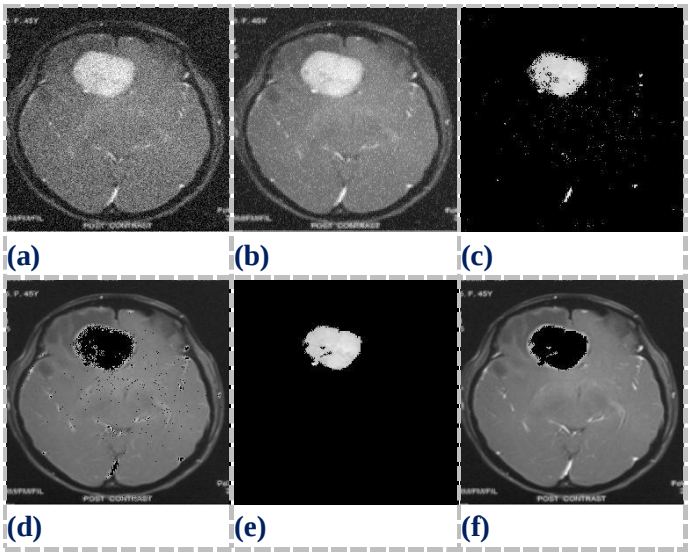

Figure 4. Img2 (A)Noisy Image, (B) Denoised image, (C) Existing K-Means segmented Tumor output, (D) Existing K-Means segmented non-Tumor output, (E) Proposed Histon based FCM segmented tumor output, (F) Proposed Histon based FCM segmented non-tumor output.

Table 2. Sensitivity, Specificity and Accuracy Measures for our proposed work.

Input Images	Sensitivity	Specificity	Accuracy
1	0.834546337	0.99527373	0.990219116
2	0.871603623	0.997486608	0.993881226
3	0.588755856	0.993146271	0.981292725
4	0.756950953	1	0.988128662
5	0.924927416	0.997813861	0.995132446
6	0.865736704	0.985906018	0.977493286

Table 3. PSNR, SSIM and MSE, metrics measures for our proposed work.

Input images	PSNR	MSE	SSIM
1	71.37515734	0.004738	0.442602877
2	69.14210699	0.007923	0.780531334
3	72.50124437	0.003656	0.412546045
4	70.37229725	0.005968	0.463971721
5	70.43645289	0.005881	0.530001656
6	77.42513233	0.001176	0.784817566

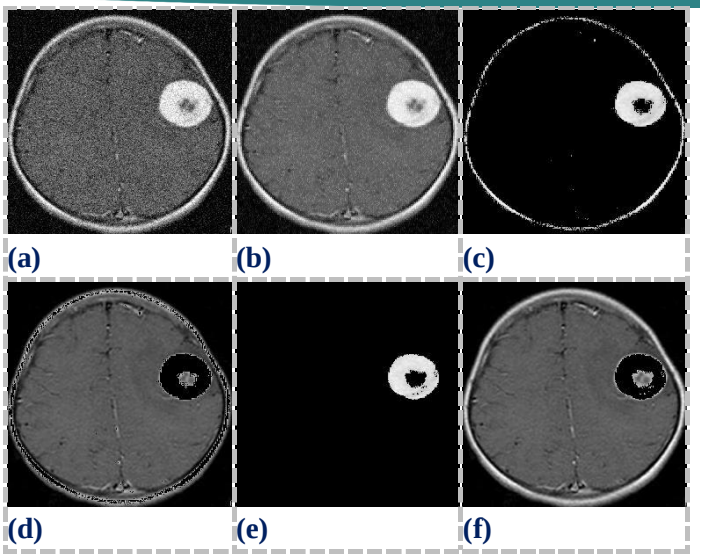

Figure 5. Img3 (A)Noisy Image, (B) Denoised image, (C) Existing K-Means segmented Tumor output, (D) Existing K-Means segmented non-Tumor output, (E) Proposed Histon based FCM segmented tumor output, (F) Proposed Histon based FCM segmented non-tumor output.

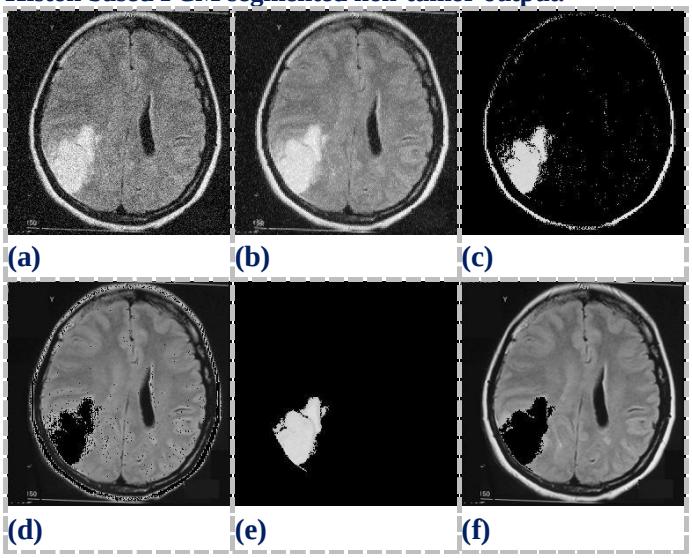

Figure 6. Img4 (A)Noisy Image, (B) Denoised image, (C) Existing K-Means segmented Tumor output, (D) Existing K-Means segmented non-Tumor output, (E) Proposed Histon based FCM segmented tumor output, (F) Proposed Histon based FCM segmented non-tumor output.

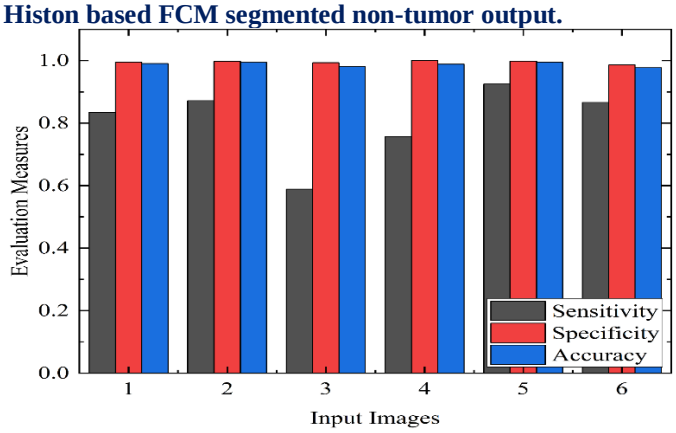

Figure 7. Graphical representation of the proposed work in terms of sensitivity, specificity and accuracy.

From Table II and Figure 7, we can understand that brain MRI image denoising and segmentation of images

DOI:https://doi.org/10.52756/ijerr.2024.v44spl.005

have good metric values for the BMRI images. Thus, it is understood that the medical images can be segmented properly by using the proposed work. The proposed method achieves the sensitivity, specificity, and accuracy measures are 80%, 99%, and 98%.

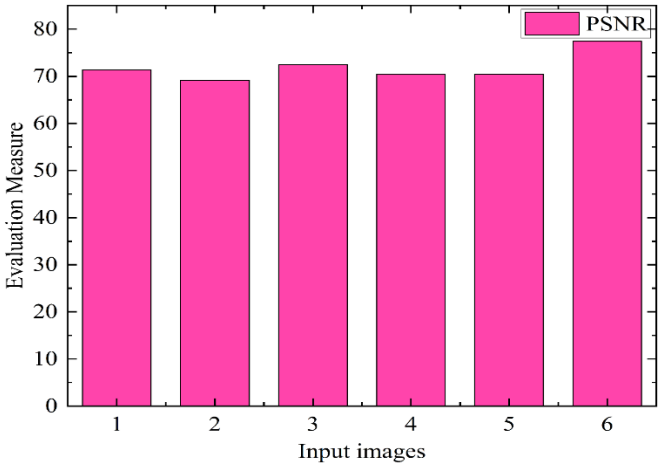

Figure 8. Graphical representation of the proposed work in terms of PSNR.

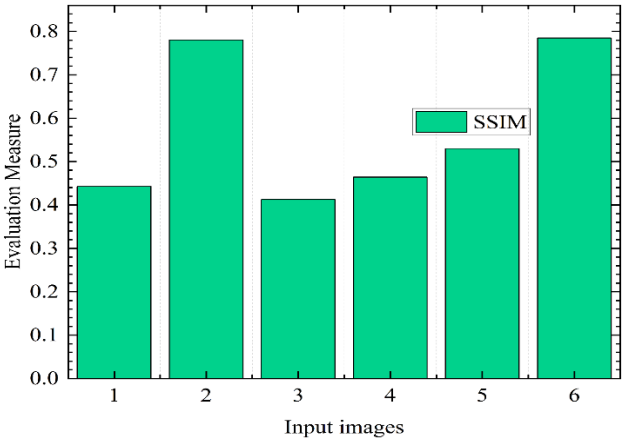

Figure 9. Graphical representation of the proposed work in terms of SSIM.

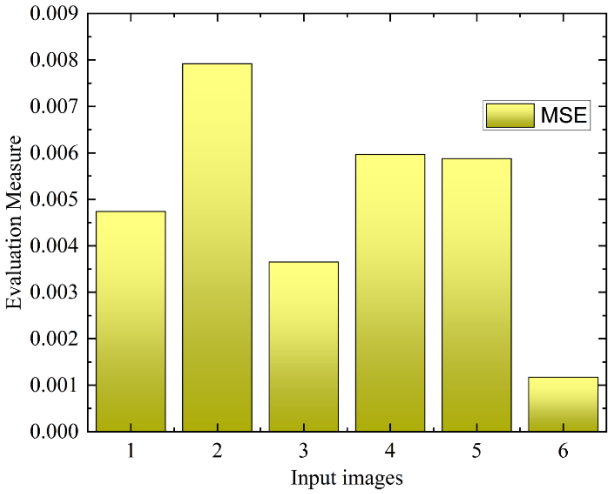

Figure 10. Graphical representation of the proposed work in terms of MSE.

From Table III and Figure 8, we can understand that brain MRI image denoising and segmentation have good metric values for BMRI images. Therefore, medical images can be segmented properly using the proposed work. Here, we have discussed the PSNR, SSIM, and MSE rates and graphically represent the proposed measures.

Table 4. Comparison of proposed and existing methods using sensitivity.

Input Images	Sensitivity for proposed Histon FCM	Sensitivity for existing k-means
1	0.834546337	0.867054828
2	0.871603623	0.937133724
3	0.588755856	0.585632483
4	0.756950953	0.664167448
5	0.924927416	0.915387806
6	0.865736704	0.87467306

Comparative analysis

In this Histon-based image denoising and segmentation work is compared with the existing K-means clustering technique to prove that the proposed work is better for image denoising and segmentation. In this section, we have used K-means clustering as the existing one. Also, we show in the following Table VI, respectively.

Table IV and Figure 11 shows that training and testing results can be taken for sensitivity. In our proposed methodology we have taken input images such as 1, 2, 3, 4 5 and 6. The input image 1 attains a sensitivity value of 0.834546337, and the input image 2 attains a sensitivity value of 0.871603623. The input image 3 attained a sensitivity value is 0.588755856. The input image 4 attained a sensitivity value is 0.756950953 and the input image 5 attained a sensitivity value of 0.924927416, and the final image 6 attained a sensitivity value of 0.865736704. When we compare the proposed Histon-based FCM results to the existing K-means clustering research, our Histon FCM technique will give the best result.

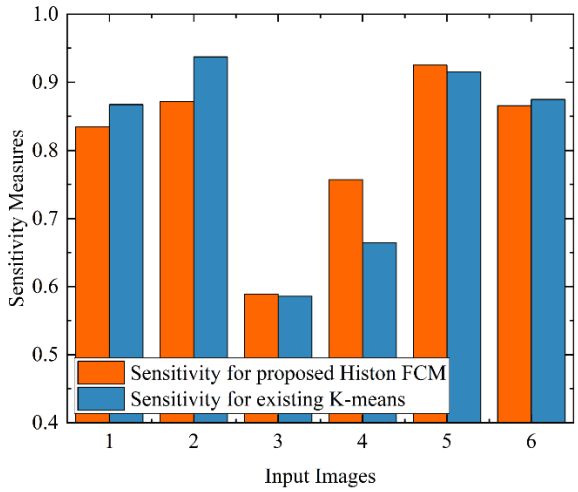

Figure 11. Comparative analysis between proposed and existing methods in terms of sensitivity.

Table V and figure 12 show that training and testing results can be taken for specificity. In our proposed

DOI:https://doi.org/10.52756/ijerr.2024.v44spl.005

methodology, we have taken input images such as 1, 2, 3 4 5 and 6. The input image 1 attained a specificity value of 0.995274 and the input image 2 attained a specificity value of 0.997487. The input image 3 attained a specificity value is 0.993146. The input image 4 attained a specificity value is 1 and the input image 5 attained a specificity value of 0.997814, and the final image 6 attained a specificity value of 0.985906. When we compare the proposed Histon-based FCM results to the existing K-means clustering, our Histon FCM technique will give the best result.

Table 5. Comparison of Proposed and Existing methods using specificity.

Input Images	Specificity for Proposed Histon FCM	Specificity for existing K-means
1	0.995274	0.961276
2	0.997487	0.971206
3	0.993146	0.981435
4	1	0.987471
5	0.997814	0.955295
6	0.985906	0.985348

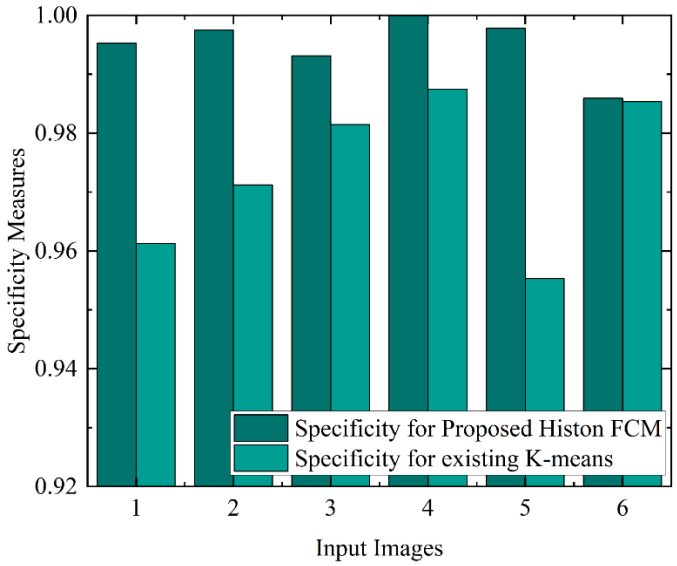

Figure 12. Comparative analysis between proposed and existing methods in terms of specificity.

Table VI and Figure 13 show that training and testing results can be taken for accuracy. In our proposed, methodology we have taken input images such as 1, 2, 3, 4 and 5. The input value attained for the accuracy value is 0.95831. The input image 2 attained an accuracy value is 0.97168. The input image 3 attained an accuracy value of 0.969833. The input image 4 attained an accuracy value is 0.97168 and the input image 5 attained an accuracy value of 0.953827, and the image 6 attained an accuracy value is 0.9776. When we compare the proposed histon-based FCM results to the existing K-Means clustering method, our Histon FCM technique will give the best result.

Table VI. Comparison of Proposed and Existing methods using accuracy.

Input Images	Accuracy for proposed Histon-FCM	Accuracy for Proposed K-means
1	0.990219	0.958313
2	0.993881	0.97023
3	0.981293	0.969833
4	0.988129	0.97168
5	0.995132	0.953827
6	0.977493	0.9776

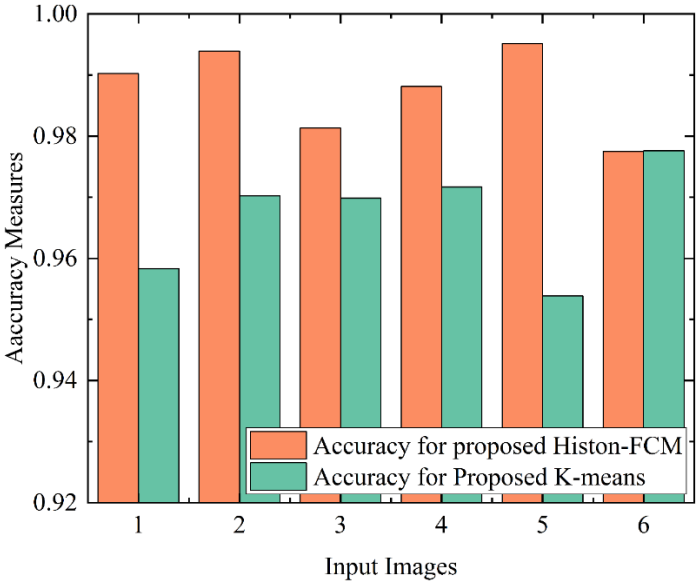

Figure 13. Comparative analysis between proposed and existing methods in terms of accuracy.

Conclusion

In this work, we proposed an effective Histon-related image denoising and segmentation algorithm that integrates Partial Differential Equation (PDE) and Generalized Cross-Validation (GCV) within the Adaptive Haar Wavelet Transform framework. The PDE is applied to address the issue of blocking artifacts and to estimate unknown coefficients, reducing noise more effectively. Additionally, GCV is used to determine the optimal denoising threshold in the tetrolet transform domain. The Fuzzy C-Means (FCM) algorithm was employed to discover association values, rather than relying solely on standardized intensity values. The experimental results show that the proposed method effectively preserves the boundaries of digital images. Performance was evaluated using Sensitivity, Specificity, Accuracy, PSNR, and SSIM metrics. Sensitivity, specificity, and accuracy measures for the proposed method were 99%, 98%, and 98%, respectively, demonstrating significant improvement over conventional methods. A comparison of the proposed Histon-related FCM approach with the

DOI:https://doi.org/10.52756/ijerr.2024.v44spl.005

existing K-means clustering method further highlighted its superiority. Graphical representations of various metrics confirm that our proposed method outperforms K-means clustering. Therefore, the proposed method proves to be a highly effective solution for both image denoising and segmentation tasks. In the future, we plan to extend this work by exploring more advanced wavelet-based techniques and optimization algorithms to further enhance the performance of image denoising and segmentation.

Acknowledgement

The authors express their gratitude to SR University and VIT-AP for their valuable support.

Conflict of Interest

The authors declare that they have no known competing financial interests or personal relationships that could have appeared to influence the work reported in this paper.

References

Abdellahoum, H., Mokhtari, N., Brahimi, A., &Boukra, A. (2021). CSFCM: An improved fuzzy C-Means image segmentation algorithm using a cooperative approach. *Expert Systems with Applications, 166*, 114063. https://doi.org/10.1016/j.eswa.2020.114063

Ai, D., Yang, J., Fan, J., Cong, W., & Wang, X. (2015). Denoising filters evaluation for magnetic resonance images. *Optik-International Journal for Light and Electron Optics, 126*(23), 3844-3850. https://doi.org/10.1016/j.ijleo.2015.07.155

Ally, N., Nombo, J., Ibwe, K., Abdalla, A. T., &Maiseli, B. J. (2021). Diffusion-driven image denoising model with texture preservation capabilities. *Journal of Signal Processing Systems, 93*(8), 937-949.https://doi.org/10.1007/s11265-020-01621-3

Aswathy, C., Sowmya, V., & Soman, K. P. (2015). Hyperspectral image denoising using low pass sparse banded filter matrix for improved sparsity based classification. *Procedia Computer Science, 58*, 26-33.
https://doi.org/10.1016/j.procs.2015.08.005

Baid, U., Ghodasara, S., Mohan, S., Bilello, M., Calabrese, E., Colak, E., & Bakas, S. (2021). The rsna-asnr-miccai brats 2021 benchmark on brain tumor segmentation and radiogenomic classification. *arXiv preprint* arXiv:2107.02314.

Bhandari, A. K., Kumar, A., Chaudhary, S., & Singh, G. K. (2016). A novel color image multilevel thresholding based segmentation using nature inspired optimization algorithms. *Expert Systems with Applications*, 1-40.
https://doi.org/10.1016/j.eswa.2016.06.044

Bhandari, A. K., Kumar, D., Kumar, A., & Singh, G. K. (2016). Optimal sub-band adaptive thresholding based edge preserved satellite image denoising using adaptive differential evolution algorithm. *Neurocomputing, 174*, 698-721.
https://doi.org/10.1016/j.neucom.2015.09.079

Cao, Y., Zhang, S., Zha, Z.J., Zhang, J., & Chen, C. W. (2014). A novel segmentation-based video-denoising method with noise level estimation. *Information Science, 281*, 507-520.
https://doi.org/10.1016/j.ins.2014.05.031

Chen, G., Zhang, P., Wu, Y., Shen, D., & Yap, P.-T. (2016). Denoising magnetic resonance images using collaborative non-local means. *Neurocomputing, 177*, 215-227.
https://doi.org/10.1016/j.neucom.2015.11.031

Cui, B., Ma, X., Xie, X., Ren, G., & Ma, Y. (2016). Classification of visible and infrared hyperspectral images based on image segmentation and edge-preserving filtering. *Infrared Physics & Technology, 81*, 79-88.
https://doi.org/10.1016/j.infrared.2016.12.010

Feng, X.C., Luo, L., Jia, X., & Wang, W. (2015). A divide-and-conquer stochastic alterable direction image denoising method. *Signal Processing, 108*, 90-101.
https://doi.org/10.1016/j.sigpro.2014.08.036

Feng, C., Zhao, D., & Huang, M. (2016). Image segmentation using CUDA accelerated non-local means denoising and bias correction embedded fuzzy c-means (BCEFCM). *Signal Processing, 122*, 164-189.
https://doi.org/10.1016/j.sigpro.2015.12.007

Fu, Y., & Dong, W. (2016). 3D magnetic resonance image denoising using low-rank tensor approximation. *Neurocomputing, 195*, 30-39.
https://doi.org/10.1016/j.neucom.2015.09.125

Gautam, S., Ahlawat, S., & Mittal, P. (2022). Binary and Multi-class Classification of Brain Tumors using MRI Images. *Int. J. Exp. Res. Rev., 29*, 1-9.
https://doi.org/10.52756/ijerr.2022.v29.001

Goel, A., Wasim, J., & Srivastava, P. (2023). A Noise reduction in the medical images using hybrid combination of filters with nature-inspired Black Widow Optimization Algorithm. *Int. J. Exp. Res. Rev., 30,* 433-441.
https://doi.org/10.52756/ijerr.2023.v30.040.

Khodabakhshi Rafsanjani, H., Sedaaghi, M. H., &Saryazdi, S. (2016). Efficient diffusion coefficient for image denoising. *Computers and Mathematics with Applications*, 1-11. https://doi.org/10.1016/j.camwa.2016.06.005

Himabindu, D. D., Pranalini, B., Kumar, M., Neethika, A., Sree N, B., C, M., B, H., & S, K. (2024). Deep CNN-based Classification of Brain MRI Images for Alzheimer's Disease Diagnosis. *International Journal of Experimental Research and Review, 41*(Spl Vol), 43-54. https://doi.org/10.52756/ijerr.2024.v41spl.004

Huang, Y., Chen, X., Zhang, J., Zeng, D., Zhang, D., & Ding, X. (2015). Single-trial ERPs denoising via collaborative filtering on ERPs images. *Neurocomputing, 149*, 914-923. https://doi.org/10.1016/j.neucom.2014.07.043

Islam, N., Shahid, Z., & Puech, W. (2016). Denoising and error correction in noisy AES-encrypted images using statistical measures. *Signal Processing: Image Communication, 41*, 15-27. https://doi.org/10.1016/j.image.2015.11.003

Jain, J., Sahu, S., & Dixit, A. (2023). Brain tumor detection model based on CNN and threshold segmentation. *Int. J. Exp. Res. Rev., 32*, 358-364. https://doi.org/10.52756/ijerr.2023.v32.031

Jalab, H. A., & Ibrahim, R. W. (2015). Fractional Alexander polynomials for image denoising. *Signal Processing, 107*, 340-354. https://doi.org/10.1016/j.sigpro.2014.06.004

han, A., Waqas, M., Ali, M. R., Altalhi, A., Alshomrani, S., & Shim, S.-O. (2016). Image de-noising using noise ratio estimation, K-means clustering and non-local means-based estimator. *Computers & Electrical Engineering*, 1-12. https://doi.org/10.1016/j.compeleceng.2015.12.019

Kollem, S. (2024). A fast computational technique based on a novel tangent sigmoid anisotropic diffusion function for image-denoising. *Soft Computing, 28*, 7501–7526. https://doi.org/10.1007/s00500-024-09628-9

Kollem, S., Reddy, K. R., & Rao, D. S. (2023). A novel diffusivity function-based image denoising for MRI medical images. *Multimedia Tools and Applications, 82*(21), 32057-32089. https://doi.org/10.1007/s11042-023-14457-3

Kollem, S., Reddy, K. R. L., & Rao, D. S. (2022). Image denoising for magnetic resonance imaging medical images using improved generalized cross-validation based on the diffusivity function. *International Journal of Imaging Systems and Technology, 32*(4), 1263-1285. https://doi.org/10.1002/ima.22681

Kollem, S., Reddy, K. R. L., & Rao, D. S. (2020). Modified transform-based gamma correction for MRI tumor image denoising and segmentation by optimized histon-based elephant herding algorithm. *International Journal of Imaging Systems and Technology, 30*(4), 1271-1293. https://doi.org/10.1002/ima.22429

Kollem, S., Reddy, K. R. L., & Rao, D. S. (2019). Denoising and segmentation of MR images using fourth order non-linear adaptive PDE and new convergent clustering. *International Journal of Imaging Systems and Technology, 29*(3), 195-209. https://doi.org/10.1002/ima.22302

Li, B., & Xie, W. (2016). Image denoising and enhancement based on adaptive fractional calculus of small probability strategy. *Neurocomputing, 75*, 704-714. https://doi.org/10.1016/j.neucom.2015.10.115

Li, X., He, H., Wang, R., & Cheng, J. (2016). Super pixel-guided nonlocal means for image denoising and super-resolution. *Signal Processing, 124*, 173-183. https://doi.org/10.1016/j.sigpro.2015.09.021

Liu, J., Wang, Y., Su, K., & He, W. (2016). Image denoising with multidirectional shrinkage in directionlet domain. *Signal Processing, 125*, 64-78. https://doi.org/10.1016/j.sigpro.2016.01.013

Lotfi, Y., & Parand, K. (2022). Efficient image denoising technique using the meshless method: Investigation of operator splitting RBF collocation method for two anisotropic diffusion-based PDEs. *Computers & Mathematics with Applications, 113*, 315-331. https://doi.org/10.1016/j.camwa.2022.03.013

Malini, S., & Moni, R. S. (2015). Image denoising using multiresolution singular value decomposition transform. *Procedia Computer Science, 46*, 1708-1715. https://doi.org/10.1016/j.procs.2015.02.114

Mishro, P. K., Agrawal, S., Panda, R., & Abraham, A. (2020). A novel type-2 fuzzy C-means clustering for brain MR image segmentation. *IEEE Transactions on Cybernetics, 51*(8), 3901-3912. https://doi.org/10.1109/TCYB.2020.2994235

Mittal, P. (2023). Wavelet transformation and predictability of Gold Price Index Series with ARMA model. *Int. J. Exp. Res. Rev., 30*, 127-133. https://doi.org/10.52756/ijerr.2023.v30.014.

Naresh, M., &Peddakrishna, S. (2023). Non-invasive near-infrared-based optical glucose detection system for accurate prediction and multi-class

classification. *Int. J. Exp. Res. Rev.*, *31*(Spl Volume), 119-130.
https://doi.org/10.52756/10.52756/ijerr.2023.v31spl.012.

Phophalia, A., & Mitra, S. K. (2014). Rough set based bilateral filter design for denoising brain MR images. *Applied Soft Computing*, *33*, 1-14. https://doi.org/10.1016/j.asoc.2015.04.005

Rafsanjani, H. K., Noori, H., & Naseri, N. (2022). Diffusion based method for impulse noise removal using residual feedback. *Computers & Mathematics with Applications*, *107*, 45-56. https://doi.org/10.1016/j.camwa.2021.12.015

Xu, S., Yang, X., & Jiang, S. (2016). A fast nonlocally centralized sparse representation algorithm for image denoising. *Signal Processing*, *131*, 99-112. https://doi.org/10.1016/j.sigpro.2016.08.006

Zhang, C., Chen, Y., Duanmu, C., & Yang, Y. (2015). Image denoising by using PDE and GCV in tetrolet transform domain. *Engineering Applications of Artificial Intelligence*, *48*, 204-229.
https://doi.org/10.1016/j.engappai.2015.10.008

Zhang, M., Jiang, W., Zhou, X., Xue, Y., & Chen, S. (2019). A hybrid biogeography-based optimization and fuzzy C-means algorithm for image segmentation. *Soft Computing*, *23*(6), 2033-2046.
https://doi.org/10.1016/j.engappai.2015.10.008

How to cite this Article:
Sreedhar Kollem, SamineniPeddakrishna, P Joel Josephson, Y Rama Lakshmanna, Garaga Srilakshmi and Sridevi Cheguri (2024).An Effective PDE-based Thresholding for MRI Image Denoising and H-FCM-based Segmentation. *International Journal of Experimental Research and Review*, *44*, 51-65.
DOI:https://doi.org/10.52756/ijerr.2024.v44spl.005